

R3DP: Real-Time 3D-Aware Policy for Embodied Manipulation

Yuhao Zhang^{1,2*}, Wanxi Dong^{3*}, Yue Shi^{1*}, Yi Liang^{1*}, Jingnan Gao¹,
Qiaochu Yang¹, Yaxing Lyu⁶, Zhixuan Liang⁴, Yibin Liu⁷, Congsheng Xu¹,
Xianda Guo^{5,2}, Wei Sui², Yaohui Jin¹, Xiaokang Yang¹, Yanyan Xu¹, and Yao Mu^{1†}

¹Shanghai Jiao Tong University ²D-Robotics ³Southern University of Science and
Technology ⁴The University of Hong Kong ⁵Wuhan University
⁶Xiamen University Malaysia ⁷Northeastern University
{yuhao_zh, muyao}@sjtu.edu.cn

<https://dazazh.github.io/r3dp-project-page/>

Abstract. Embodied manipulation requires accurate 3D understanding of objects and their spatial relations to plan and execute contact-rich actions. While large-scale 3D foundation models provide strong priors, their computational cost incurs prohibitive latency for real-time control. We propose **Real-time 3D-aware Policy (R3DP)**, which integrates powerful 3D priors into manipulation policies without sacrificing real-time performance. A core innovation of R3DP is the asynchronous fast-slow collaboration module, which sophisticatedly integrates large-scale 3D model’s priors into the policy without compromising real-time performance. The system queries the pre-trained slow system (VGGT) only on sparse key frames, while simultaneously employing a lightweight Temporal Feature Prediction Network (TFPNet) to predict features for all intermediate frames. By leveraging historical data to exploit temporal correlations, TFPNet explicitly improves task success rates through consistent feature estimation. Additionally, we introduce a Multi-View Feature Fuser (MVFF) that aggregates features across views by explicitly incorporating camera intrinsics and extrinsics. R3DP offers a plug-and-play solution for integrating 3D foundation models into real-time inference systems. We evaluate R3DP against multiple baselines across different visual configurations. R3DP effectively harnesses large-scale 3D priors to achieve superior results, outperforming single-view and multi-view DP by 32.9% and 51.4% in average success rates. Furthermore, by decoupling heavy 3D understanding from policy execution, R3DP achieves a 44.8% reduction in inference time compared to a naive DP+VGGT integration.

Keywords: Imitation Learning · Diffusion Policy · 3D Foundation Model

1 Introduction

Humans naturally perceive and reason about the world in 3D or 4D, leveraging spatial perception and temporal continuity to perform complex manipulation

* Co-first authors, equal contribution. † Corresponding author.

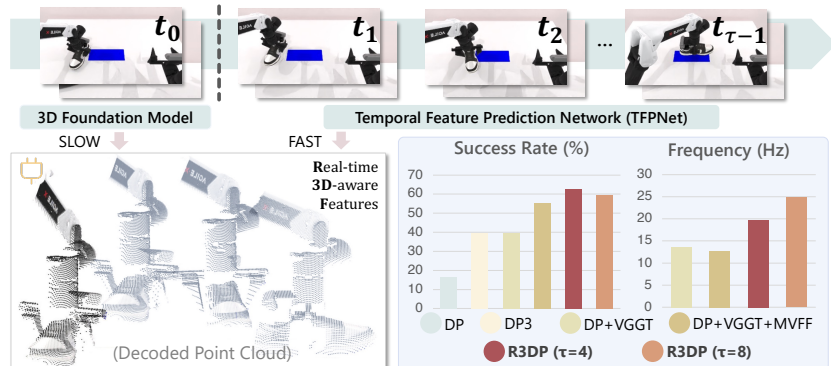


Fig. 1: Key modules and performance of R3DP. Our framework explicitly integrates 3D priors from large-scale foundation models (e.g., VGGT) via an asynchronous fast-slow collaboration mechanism. Overall, R3DP achieves real-time, 3D-aware inference, significantly improving both manipulation success rates and processing frequency.

tasks. However, current learning-based imitation methods [6, 27, 30] for embodied manipulation often *i*) lack an explicit, native 3D representation of the scene, relying primarily on 2D visual features that are weakly grounded in geometry, and *ii*) struggle to effectively and efficiently model temporal context from historical observations, achieving limited success.

A straightforward way to compensate for the lack of 3D awareness is to augment RGB observations with additional modalities such as depth maps or point clouds. Prior works [22, 42] along these lines have shown that the injection of 3D information can indeed improve manipulation performance. However, the reliance on extra sensors or calibrated rigs of these methods increases system complexity. Such dependency leaves the system vulnerable to noise on transparent, reflective, or textureless surfaces, thereby limiting their practicality for real-world large-scale deployment. Moreover, embodied manipulation is inherently sequential that interaction trajectories naturally contain rich temporal cues about contacts, occlusions, and object motion. Several approaches attempt to exploit this by adding recurrent modules or memory mechanisms [24, 26] to imitation policies. But temporal context is often treated as an implicit hidden state, making it difficult to enforce spatial-temporal consistency or maintain a stable 3D understanding of the scene over long horizons.

Recent progress has seen large-scale 3D vision foundation models [33, 38] rapidly develop, which presents good opportunities to obtain 3D priors directly from RGB inputs. These models offer a promising path to endow embodied policies with 3D spatial understanding, and without requiring additional depth or point cloud sensors. Unfortunately, their high computational cost makes per-frame inference far too slow for real-time robot control, especially in multi-view settings. Therefore, it is essential to design an approach that *effectively and efficiently integrates these large-scale 3D priors with temporal context* into embodied manipulation policies, enabling 3D-aware control under real-time constraints.

We propose R3DP, a real-time 3D-aware policy for embodied manipulation that aggregates both 3D priors and temporal context information. An overview of R3DP and its performance are shown in Fig. 1. Basically, we integrate the 3D intermediate features from the large 3D foundation model VGGT [33] into the diffusion policy [6]. However, running such a large 3D model on every frame is prohibitively slow. Therefore, to satisfy real-time constraints, we introduce an Asynchronous Fast–Slow Collaboration (AFSC) module with a lightweight Temporal Feature Prediction Network (TFPNet) for fast feature inference. AFSC queries VGGT only on sparse key frames and quickly derives features for the other frames using TFPNet. TFPNet is pre-trained to predict the current frame from historical frames, not only helping AFSC satisfy the requirement of real-time 3D prior injection but also providing additional temporal context to the policy. Furthermore, in addition to leveraging single-view 3D priors, we introduce a dedicated Multi-View Feature Fuser (MVFF) to explicitly aggregate multi-view features into a consistent 3D representation. MVFF leverages camera intrinsics and extrinsics to guide cross-view fusion, inspired by [16, 18].

The contributions of this work can be summarized as follows:

- **A Plug-and-Play 3D-Aware Policy Paradigm:** We propose R3DP, a real-time framework that seamlessly integrates 3D foundation model features into 2D image-based policies. This architecture endows robots with robust spatial perception while preserving the inherent strengths of 2D policy.
- **Efficient Asynchronous Inference Mechanism:** To bypass 3D computational bottlenecks, we introduce an Asynchronous Fast–Slow Collaboration (AFSC) system, sophisticatedly integrating high-latency 3D features into real-time policies. This fast-slow collaboration ensures robust responsiveness during dynamic manipulation tasks.
- **Geometry-Informed Multi-View Feature Fusion:** We introduce a Multi-View Feature Fuser (MVFF) that explicitly leverages camera intrinsics and extrinsics to aggregate features across multiple perspectives. This ensures spatial consistency and enhances the policy’s robustness in complex environments with occlusions.
- **Extensive Validation of Effectiveness and Efficiency:** We extensively evaluate R3DP across diverse tasks, visual configurations, and baselines. R3DP improves average success by 32.9% and 51.4% over single-view and multi-view DP, respectively, and reduces inference latency by 44.8% compared to the naive DP+VGGT integration via asynchronous fast–slow pipeline.

2 Related Work

2D-based Imitation Learning. Recent advances in imitation learning have demonstrated strong policy performance using purely 2D visual inputs. Notable approaches [2, 3, 6, 11, 19, 21, 45] leverage powerful visual encoders and generative policies to learn from demonstrations. While effective on many manipulation tasks, these methods typically rely on RGB observations rather than explicitly reasoning about the underlying 3D scene. As a result, they often struggle in tasks

requiring spatial reasoning, depth understanding, or handling occlusions. Moreover, multi-view inputs are often fused via simple concatenation or flattening, without leveraging camera geometry or enforcing spatial consistency.

3D-Aware Imitation Learning. To overcome the limitations of 2D-only perception, several methods [12, 14, 18, 20, 29, 40, 41] use RGB-D, point cloud representations, or voxel-based representations to enhance spatial awareness in robotic tasks. However, such approaches require additional depth sensors, which are prone to noise, particularly in challenging conditions, such as those involving transparent or reflective surfaces. Furthermore, real-world deployment may be constrained by hardware costs or limited sensor coverage. In contrast, our work avoids explicit depth sensing and instead builds upon 3D visual foundation models to extract geometry-aware features directly from RGB inputs.

Imitation Policies with Large-scale 3D Prior. Recent methods have explored using pre-trained 3D foundation models [4, 8, 10, 13, 15, 31–37, 43, 44] to provide strong priors for manipulation. These methods [1, 17, 28] simply fused pre-trained features into imitation policies, whereas methods like eVGGT [7] use distillation to make VGGT efficient for robotic policy inference. These approaches do enhance spatial understanding and geometry-aware action generation. However, integrating such large-scale priors introduces significant challenges: these models often suffer from *scale shifting*—a mismatch in feature magnitudes over time that degrades policy stability. More critically, these models typically incur significant *inference latency* in real-world deployment. Furthermore, multi-view information is often merged heuristically, without explicit encoding of camera intrinsics or extrinsics. To address these issues while maintaining spatial-temporal consistency, we introduce a *fast-slow system* inspired by prior temporal models [9], which explicitly separates transient local features from relatively stable 3D scene representations, enabling the policy to maintain geometric consistency while preserving real-time performance.

3 Preliminary

Imitation Learning. Imitation learning aims to acquire a control policy by mimicking expert behavior from demonstrations. Given an expert dataset $\mathcal{D} = \{(s_i, a_i, s'_i)\}_{i=1}^N$, where $s_i \in S$ is the state, $a_i \in A$ is the action taken in state s_i , and s'_i is the resulting next state, the goal of imitation learning is to obtain a policy $\pi : S \rightarrow A$ that reproduces the expert’s behavior.

Diffusion Policy. Diffusion policy [6] (DP) is a visuomotor imitation learning method that models the distribution of future action sequences with a conditional Denoising Diffusion Probabilistic Model (DDPM). Instead of directly regressing actions in an autoregressive manner, DP learns to iteratively denoise a noisy action sequence into a feasible plan conditioned on the current observation. Concretely, at time step t , the policy conditions on an observation O_t (e.g., stacked RGB frames and proprioception) and predicts a future action sequence A_t^0 . DP trains a parameterized noise prediction network ϵ_θ and applies it in a

k -step iterative denoising process:

$$A_t^{k-1} = \alpha(A_t^k - \gamma\epsilon_\theta(O_t, A_t^k, k) + \mathcal{N}(0, \sigma^2 I)), \quad (1)$$

where A_t^k is the randomly sampled Gaussian noise, A_t^0 is the expected noise-free action output at time t , O_t is the observation data used as the condition, γ is the learning rate, and $\mathcal{N}(0, \sigma^2 I)$ represents the Gaussian noise added during the iteration. To obtain the optimal parameters θ , the training loss is defined as:

$$\mathcal{L}_{DP} = \mathbb{E}_{(O_t, A_t^0), k, \epsilon} [\|\epsilon - \epsilon_\theta(O_t, A_t^0 + \epsilon_k, k)\|_2^2], \quad (2)$$

where k is the randomly chosen denoising iteration step, and ϵ^k is the random noise with a variance matching the k -step sampling.

Projective Positional Encoding (PRoPE). Existing methods encode only SE(3) extrinsic pose T_i^{cw} , fundamentally neglecting intrinsic parameters K_i and failing on cameras with varying focal lengths. Projective Positional Encoding (PRoPE) [16] addresses this by modeling complete frustum geometry via relative projective transformations. The core innovation of PRoPE lies in modeling inter-camera relationships through relative projective transformations:

$$\tilde{\mathbf{P}}_{i,j} = \begin{bmatrix} \mathbf{K}_i & \mathbf{0} \\ \mathbf{0} & 1 \end{bmatrix} \mathbf{T}_i^{cw} (\mathbf{T}_j^{cw})^{-1} \begin{bmatrix} \mathbf{K}_j^{-1} & \mathbf{0} \\ \mathbf{0} & 1 \end{bmatrix}. \quad (3)$$

PRoPE is injected via GTA-style [23] attention using per-token block-diagonal transformation:

$$D_t^{\text{PRoPE}} = \begin{bmatrix} D_t^{\text{Proj}} & \mathbf{0} \\ \mathbf{0} & D_t^{\text{RoPE}} \end{bmatrix} \in \mathbb{R}^{d \times d}, \quad (4)$$

$$D_t^{\text{Proj}} = I_{d/8} \otimes \tilde{\mathbf{P}}_{i(t)} \in \mathbb{R}^{\frac{d}{2} \times \frac{d}{2}}, \quad (5)$$

$$D_t^{\text{RoPE}} = \begin{bmatrix} \text{RoPE}_{d/4}(x_t) & \mathbf{0} \\ \mathbf{0} & \text{RoPE}_{d/4}(y_t) \end{bmatrix} \in \mathbb{R}^{\frac{d}{2} \times \frac{d}{2}}. \quad (6)$$

This formulation guarantees global frame invariance, reduces to SE(3) encoding when intrinsics are shared, and degrades gracefully to RoPE for tokens within identical views.

4 Methodology

Although diffusion policy is powerful in modeling complex action distributions, it faces several key limitations when directly applied to 3D robotic manipulation: **i) Lack of 3D perception.** Standard diffusion policy and its variants typically rely on generic 2D visual encoders (e.g., ResNet) to extract observation features, and thus lack explicit 3D spatial perception of the scene; **ii) Implicit multi-view fusion.** Standard implementation of diffusion policy uses simple feature concatenation for implicit fusion of multiple views. This implicit fusion does not explicitly encode camera intrinsics and extrinsics, and therefore underutilizes the underlying geometric structure across views.

The overall architecture of R3DP is illustrated in Figure 2. Compared to standard 2D image-based imitation policies, R3DP is designed around several key

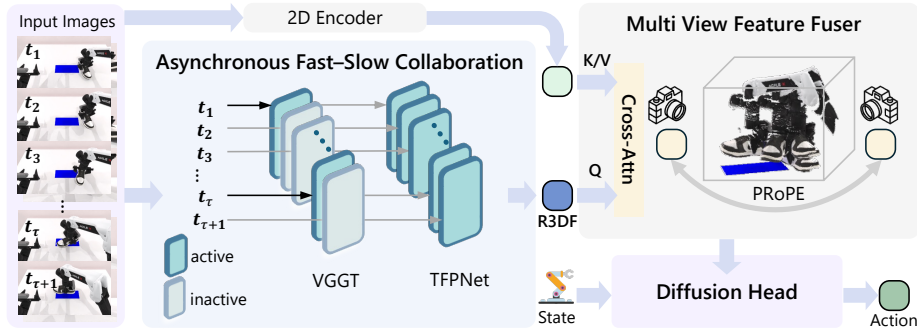


Fig. 2: Overview of the R3DP architecture. R3DP serves as a 3D-aware perception module that seamlessly replaces visual encoders in existing imitation learning frameworks. Within the AFSC module (4.1), sparse keyframes are processed by a 3D foundation model (VGGT), while intermediate frames are handled by our TFPNet (4.2) for real-time temporal reasoning. MVFF module (4.3) leverages cross-attention with PRoPE to fuse 2D-3D features into consistent multi-view representations for control.

aspects: 3D-aware perception, real-time feasibility, temporal context assistance, and explicit multi-view fusion. Concretely, it consists of three core components. First, the Asynchronous Fast-Slow Collaboration (AFSC) module injects 3D priors into the policy by leveraging a large 3D vision foundation model (VGGT) as a slow branch that processes sparse key frames and produces 3D-aware features. Second, the lightweight Temporal Feature Prediction Network (TFPNet) acts as the fast branch. It is pre-trained to predict current-frame features from historical observations, both propagating VGGT features to intermediate frames and providing explicit temporal modeling in real time. Third, a Multi-View Feature Fuser (MVFF) explicitly aggregates per-view features using camera intrinsics and extrinsics to form a consistent 3D-aware representation across viewpoints.

4.1 Asynchronous Fast-Slow Collaboration

Directly applying large 3D vision models at every frame to extract 3D features cannot meet the real-time control requirements of embodied manipulation. To enable efficient 3D perception, we propose an AFSC module that collaborates a slow 3D backbone with a fast temporal predictor to predict 3D features.

AFSC treats a large 3D vision foundation model as the slow system that takes current multi-view RGB images every τ inferences, and computes high-fidelity Slow 3D-aware Features (S3DF). Meanwhile, AFSC takes a lightweight Temporal Feature Prediction Network (TFPNet) as the fast system that propagates these features to every intermediate frame using historical context to predict the Real-time 3D-aware Features (R3DF). Specifically, the slow and fast systems Φ_{slow} and Φ_{fast} , can be represented as:

$$\begin{aligned} \Phi_{\text{slow}} &: \mathbf{I}_{i_0} \xrightarrow{\text{VGGT}} F_{i_0}^{\text{S3D}}, \\ \Phi_{\text{fast}} &: (F_{i-1}^{\text{R3D}}, \mathbf{I}_i) \xrightarrow{\text{TFPNet}} F_i^{\text{R3D}}, \end{aligned} \quad (7)$$

where $i \in (i_0, i_0 + \tau)$ is the current inference iteration, $\mathbf{I}_i \in \mathbb{R}^{V \times 3 \times H \times W}$ is multi-view RGB frame of iteration i , F_i^{S3D} , F_i^{R3D} are slow and real-time features, respectively. In this way, AFSC efficiently injects 3D priors to meet the real-time requirements of embodied manipulation.

After obtaining per-view feature, we explicitly aggregate features across views (as in Sec. 4.3), yielding a fused 3D-aware visual representation. We feed the derived features into the diffusion denoiser to generate the future action sequence. To expose longer temporal dependencies during training while keeping computation affordable, we modify the diffusion policy sampler so that each training tuple contains eight frames uniformly spaced by a fixed stride of eight timesteps (instead of three consecutive frames). This yields an effective temporal window of $8 \times 8 = 64$ frames, suitable for common manipulation horizons and aligned with AFSC’s single-key-frame schedule. Within each tuple, the first frame is processed by VGGT to produce the initial S3DF; subsequent frames are updated by TFPNet to produce ordered R3DF. Training is performed serially within each tuple but in parallel across batches. In this stage, gradients are only updated for the diffusion head, as the vision backbones (VGGT and TFPNet) remain frozen, and the entire framework is trained end-to-end with a unified diffusion loss.

4.2 Temporal Feature Prediction Network

To bridge the gap between 3D vision backbones and real-time embodied manipulation, we pre-train a lightweight Temporal Feature Prediction Network (TFPNet) that leverages historical-frame 3D-aware features to predict the current-frame feature online in real time.

TFPNet is trained by distilling supervision from a large 3D vision foundation model (VGGT). For each episode, we sample 4 frames $\{t_0, t_1, t_2, t_3\}$ in chronological order, with a random interval of 1–8 frames between them to simulate the temporal gap that typically occurs between two inference steps in manipulation (i.e., after an action chunk is executed). These ordered frames form one training tuple. During training, all frames are first processed by VGGT to obtain the ground-truth 3D features F^{S3D} , which are the unified tokens extracted from 24 layers for VGGT’s dense output as follows:

$$F^{S3D} = \text{VGGT}(\mathbf{I}_{t_0}). \quad (8)$$

The TFPNet then receives the VGGT feature from the first frame and iteratively predicts features for subsequent frames. Then R3DF is predicted by the

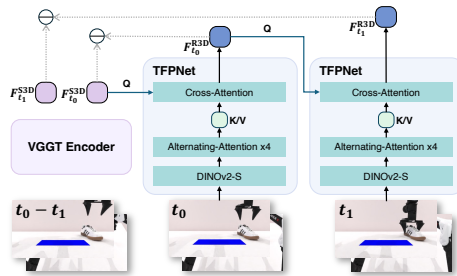


Fig. 3: Architecture and training objective of TFPNet. For clarity, we show the unrolled structure for the first two timesteps; in practice, the network is trained over a sequence of four timesteps. TFPNet leverages historical information to augment current observations, enabling 3D-aware control with real-time inference efficiency.

TFPNet \mathcal{G} of frame t as follows:

$$F_{t_k}^{\text{R3D}} = \begin{cases} \mathcal{G}(F^{\text{S3D}}, \mathbf{I}_{t_0}), & k = 0, \\ \mathcal{G}(F_{t_{k-1}}^{\text{R3D}}, \mathbf{I}_{t_k}), & k \in \{1, 2, 3\}, \end{cases} \quad (9)$$

where $\mathbf{I}_t \in \mathbb{R}^{V \times 3 \times H \times W}$ is multi-view RGB view of timestep t , F_t^{S3D} , F_t^{R3D} are slow and real-time features of timestep t .

As shown in Figure 3, TFPNet follows a compact, 3D-aware design. Each view is first encoded by a DINOv2-S [25] backbone to produce 2D features, and then passed through four Alternating-Attention (AA) Transformer [33] blocks to perform cross-view aggregation. Finally, the aggregated per-view tokens attend to the historical feature (e.g., F_{t-1}^{R3D}) via cross-attention, injecting temporal priors to stabilize optimization and improve long-horizon reasoning.

The TFPNet is pre-trained using a cosine similarity loss between the predicted features f_t and the VGGT features F_t as follows:

$$\mathcal{L}_{\text{TFP}} = \sum_{i=0}^3 (1 - \cos(F_t^{\text{S3D}}, F_t^{\text{R3D}})). \quad (10)$$

This objective encourages TFPNet to produce more accurate features leveraging temporal context. Besides, the lightweight design of TFPNet enables real-time inference. After pre-training, TFPNet is inserted into our AFSC module as the fast system, enabling real-time inference.

4.3 Multi-View Feature Fuser

The cameras mounted on the robot wrist or fixed in the background can inherently provide ground-truth extrinsic parameters. Inspired by this observation, we design the MVFF module to leverage these parameters for enhancing multi-view 3D representations. Although the VGGT backbone can implicitly infer camera parameters from its feature representations, the estimated values remain imperfect. To fully exploit the reliable ground-truth camera information, the MVFF module explicitly injects camera parameters into the model, thereby achieving a more consistent and effective fusion of multi-view 2D and 3D features.

The VGGT feature serves as a unified multi-view representation; however, it still preserves view-specific properties, since each view can be independently decoded into a distinct depth map. In parallel, each view’s image is processed by a ResNet encoder to obtain 2D features. In detail, We first apply cross-attention to fuse the 2D and 3D representations for each view, obtaining a per-view 2D–3D hybrid feature. Then, a PRoPE module, which follows the RoPE-style relative positional encoding to avoid dependence on absolute order, explicitly incorporates camera intrinsics and extrinsics to enhance multi-view feature aggregation. Formally, the overall process is expressed as:

$$Q = W_Q F_t^{2\text{D}}, K = W_K F_t^{\text{R3D}}, V = W_V F_t^{\text{R3D}}, \quad (11)$$

$$\tilde{F}_t = \text{softmax}\left(\frac{QK^\top}{\sqrt{d}}\right)V, \quad (12)$$

$$F_t^{\text{fused}} = \text{PRoPE}\left(\tilde{F}_t, K_t, E_t\right), \quad (13)$$

where K_t and E_t denote the camera intrinsics and extrinsics, respectively. The fused feature F_t^{fused} serves as the final visual embedding that conditions the diffusion model during policy learning.

5 Experiments

5.1 Experimental Setup on Simulation Benchmark

Simulated Environments. We conduct experiments on 10 representative tasks of RoboTwin [5], a scalable dual-arm manipulation benchmark with diverse tasks and unified protocols. Among them, 9 tasks are drawn directly from the original RoboTwin benchmark. Meanwhile, we also include an additional task, *Tube Insert*, to specifically evaluate the capability of 3D foundation model-based policies for handling transparent-object manipulation. Detailed task descriptions are provided in the supplementary materials.

Baselines. Our primary baseline is the Diffusion Policy (DP), evaluated under both single-view and multi-view settings. In the RoboTwin environment, the single-view configuration uses only the head camera, whereas the multi-view configuration uses both the head and front cameras. We choose DP as the baseline because it is a lightweight visuomotor imitation model that relies solely on 2D image inputs and lacks explicit 3D perception or temporal modeling. This makes it an ideal testbed for assessing the benefits introduced by our R3DP framework.

In addition, we include 3D Diffusion Policy (DP3) [41] as a depth-aware baseline. DP3 operates on head-view point cloud inputs and thus requires depth information and object bounding boxes for cropping. In simulation, where ground-truth depth and bounding boxes are available, DP3 performs competitively. However, its performance degrades significantly when depth is noisy or incomplete. To further evaluate robustness under realistic sensing conditions, we also compare Depth Anything v2 (DA2) [39] + DP3, where DA2 predicts depth maps that are back-projected into point clouds for DP3.

We also introduce π_0 [3] as a representative VLA (Vision-Language-Action) baseline. Utilizing a large-scale VLM (Vision-Language Model) as its backbone and having been pre-trained on massive datasets, π_0 exhibits exceptional generalization capabilities. To align with the experimental settings of imitation policies, we fine-tuned a separate model for each task from the π_0 -base using LoRA.

Evaluation Metrics. To ensure a fair comparison across various models and tasks, all methods are evaluated using checkpoints from a consistent training stage under identical environmental configurations. For each task and each model, we evaluate the selected checkpoint in the RoboTwin environment and measure performance by computing the success rate over 100 execution trials.

In addition, we measure the inference efficiency of each policy using the observation encoding time, defined as the average latency from raw multi-view images to the final fused feature used to condition the policy head. This metric captures the overall perception latency and serves as a key indicator for validating the inference speed advantage of our R3DP framework.

Table 1: Task success rates on RoboTwin benchmark. We report single-view Diffusion Policy (DP-single), multi-view Diffusion Policy (DP-multi), DP3, DP3+DA2, π_0 and Diffusion Policy with R3DP-enhanced feature (**R3DP**). For R3DP, we select $\tau = 4$ and $\tau = 8$. Note that τ can serve as a configurable hyperparameter at inference time to achieve a trade-off between inference speed and success rate.

Task	DP-single	DP-multi	DP3	DP3-DA2	π_0	R3DP ($\tau=4$)	R3DP ($\tau=8$)
Block Hammer Beat	0%	0%	49%	7%	47%	77%	77%
Block Handover	1%	2%	48%	31%	71%	95%	93%
Bottle Adjust	55%	6%	75%	37%	46%	62%	56%
Blocks Stack Easy	6%	7%	26%	3%	79%	69%	62%
Shoe Place	45%	19%	49%	34%	71%	72%	68%
Container Place	48%	14%	89%	37%	77%	63%	54%
Dual Shoes Place	6%	9%	11%	0%	29%	24%	20%
Diverse Bottles Pick	16%	17%	34%	7%	47%	31%	32%
Put Apple Cabinet	92%	38%	98%	94%	64%	100%	98%
Tube Insert	92%	64%	97%	32%	68%	97%	97%
Average	36.1%	17.6%	57.6%	28.2%	59.9%	69.0%	65.7%

Table 2: Average latency from raw multi-view images to fused features, averaged over four tasks (Blocks Stack Easy, Block Hammer Beat, Shoe Place, Diverse Bottles Pick) experimented in the ablation study.

Latency (ms \downarrow)	DP+VGGT	DP+VGGT+MVFF	R3DP($\tau = 4$)	R3DP($\tau = 8$)
Obs. Encoder	73.1	78.3 (\uparrow 7.1%)	50.5 (\downarrow 30.9%)	40.3 (\downarrow 44.8%)
Action Expert	56.6	57.7	55.3	56.7

Implementation Details. For R3DP, we train the model with $\tau = 8$ for 600 epochs on 4 NVIDIA 4090s using Adam (lr = 2e-5, batch size = 8). The universal TFPNet is trained on 8 NVIDIA A800s. For any part that involves the output of VGGT, we use bfloat16 precision to accelerate training and evaluation.

5.2 Results on Simulation Benchmark

Quantitative Results. We first compared R3DP against two simple yet efficient policies: the single-view Diffusion Policy and the multi-view Diffusion Policy. As shown in Table 1, R3DP achieves consistent and remarkable performance gains across all ten manipulation tasks in the RoboTwin benchmark. In tasks requiring fine-grained 3D reasoning and precise coordination—such as *Block Hammer Beat*, *Blocks Stack Easy*, and *Block Handover*—R3DP attains success rates of 77%, 69%, and 95%, respectively, representing dramatic improvements over the single-view Diffusion Policy baseline (0%, 6%, and 1%). Even in simpler placement or alignment tasks, including *Shoe Place* and *Container Place*, our framework consistently improves accuracy by more than 15%.

Interestingly, we observe that the Diffusion Policy with multi-view inputs (denoted as DP-multi) exhibits lower success rates than the single-view DP. This indicates that traditional Diffusion Policy struggles to effectively fuse multi-view information, as its naïve combination of multiple perspectives fails to leverage the rich 3D cues fully. In contrast, R3DP employs the MVFF (Multi-View Feature

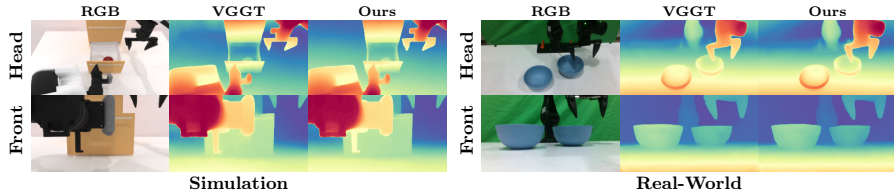


Fig. 4: Visualization of depth maps decoded from VGGT features and from our TFPNet-predicted features passed through VGGT’s depth decoder. The close visual agreement indicates that our lightweight TFPNet effectively captures information generated by 3D foundation model in both simulation and real-world experiments.

Fuser) module, which explicitly models cross-view interactions and effectively extracts 3D features from multi-view inputs. Overall, R3DP achieves an average success rate of 69.0%, outperforming the single-view and multi-view Diffusion Policies by 32.9% and 51.4%, respectively.

We observed that the DP3 baseline achieves a significantly high success rate, which we hypothesize is due to its reliance on ground-truth depth data in simulation. However, when noisy point clouds generated by depth estimation models are used, its performance drops drastically. Compared to the DP3 baselines, our model surpasses DP3 and DP3 + DA2 by 11.4% and 40.8%. Moreover, we found that our model outperforms π_0 (with an average success rate of 59.9%) on the majority of tasks, potentially because the limited data volume poses a significant challenge for a general-purpose VLA model to effectively converge on or fit the task-specific distributions.

These results validate the core novelty of R3DP: by asynchronously coupling a pretrained large-scale 3D backbone (VGGT) with a lightweight temporal prediction network, the policy can efficiently exploit rich geometric priors while still meeting real-time control constraints. Moreover, by visualizing the feature maps predicted by TFPNet and comparing them with those produced by VGGT in Figure 4, we observe highly consistent 3D representations, confirming that our lightweight network successfully captures VGGT-like 3D cues and thereby enables such performance gains with a much smaller model.

Inference Speed. We further evaluate the runtime efficiency of R3DP. While incorporating the fast-slow collaboration module inevitably introduces additional computation compared to the original DP, R3DP remains significantly faster than the naïve DP+VGGT combination, which queries the large 3D backbone at every frame. As shown in Table 2, R3DP achieves real-time 3D feature processing latency at 40.3ms (vs. 73.1ms for DP+VGGT and 78.3ms for DP+VGGT+MVFF), demonstrating that our asynchronous design effectively balances accuracy and latency, enabling practical deployment in real-world robotic control.

Configurable Efficiency and Robustness. R3DP supports real-time 3D feature processing with high flexibility. Our AFSC allows users to adjust the window size parameter τ to optimize inference latency based on hardware constraints. Notably, R3DP exhibits remarkable robustness to changes in τ ; for instance, when τ increases from 4 to 8, the encoding latency reduces by 20.2% while maintaining a highly stable success rate (with a negligible fluctuation of only

Table 3: Ablation study on the effectiveness of key components. We progressively add the 3D foundation model (VGGT), Multi-View Feature Fusion (MVFF), and AFSC to the baseline (DP-multi). The final model with all components denotes **R3DP**.

Task	DP-multi	DP+VGGT	DP+VGGT+MVFF	R3DP
Blocks Stack Easy	7%	30%	51%	69%
Block Hammer Beat	0%	44%	74%	77%
Shoe Place	19%	55%	66%	72%
Diverse Bottles Pick	17%	30%	30%	31%
Average	10.8%	39.8%	55.3%	62.3%

3.3%). This suggests that τ can be tuned at deployment to optimize real-time performance without retraining or sacrificing policy reliability. Full experiments on different τ are shown in the supplementary materials.

5.3 Ablation Study

The Table 3 reports ablation results that validate the effectiveness of each key component in the proposed R3DP framework. We systematically examine the effectiveness of the 3D foundation model VGGT, the Multi-View Feature Fuser (MVFF), and the Asynchronous Fast-Slow Collaboration (AFSC) module.

Effectiveness of 3D Foundation Model. We first evaluate the impact of augmenting Diffusion Policy with the pretrained VGGT backbone, which we denote as DP+VGGT. In this setting, each frame is independently processed by VGGT without temporal modeling, allowing us to isolate the effect of 3D priors. We use a geometry-agnostic multi-level attention-based fusion module, rather than MVFF, to fuse 2D and 3D features. Although no historical information or camera parameters are used, VGGT provides strong 3D-awareness that substantially improves spatial reasoning and manipulation precision.

As shown in Table 3, using the 3D features obtained from VGGT (DP+VGGT) increased the average success rate of DP-multi from 10.8% to 39.8%. Specifically, for the geometry-aware tasks such as *Blocks Stack Easy* and *Block Hammer Beat*, the success rates of DP-multi were only 7% and 0%, respectively. After injecting VGGT features, the success rates of these two tasks increased to 30% and 44%, which is sufficient to demonstrate that 3D foundation models can serve as powerful sources of geometric priors to enhance policy perception.

Effectiveness of MVFF. Building on the VGGT-enhanced baseline, we further introduce the Multi-View Feature Fuser (MVFF) to explicitly leverage camera intrinsics and extrinsics for geometry-aware cross-view feature alignment, enabling the policy to more effectively integrate complementary visual cues across different viewpoints. As shown in Table 3, compared to DP+VGGT, integrating MVFF (DP+VGGT+MVFF) yields a clear performance gain, with the average success rate improving from 39.8% to 55.3%. This demonstrates that MVFF effectively strengthens the multi-view representation rather than merely depending on VGGT’s 3D priors. The improvement is particularly pronounced in geometry-sensitive tasks, such as *Blocks Stack Easy* (from 30% to 51%) and *Block Hammer Beat* (from 44% to 74%), where accurate multi-view spatial reasoning is crucial.

Effectiveness of AFSC. Finally, we equip the model with the Asynchronous Fast–Slow Collaboration (AFSC) mechanism, which we denoted as R3DP, to inject temporal information on top of VGGT. While the VGGT-only variant introduces 3D priors at each frame, AFSC complements it by modeling temporal dependencies and maintaining feature consistency across time.

As shown in Table 3, the integration of AFSC significantly improves task success rates. For example, *Blocks Stack Easy* increases from 51% to 69%, and *Block Hammer Beat* improves from 74% to 77%. The average performance across all tasks increases from 55.3% to 62.3%, demonstrating the effectiveness of the AFSC module in enhancing overall task performance. Moreover, as shown in Table 2, R3DP substantially reduces inference latency. With R3DP ($\tau = 4$), the average inference time of observation encoding across tasks drops to 50.5ms from 78.3ms in DP+VGGT+MVFF, resulting in a significant speedup of 35.5%. The real-time performance is further improved with $\tau = 8$, where the average latency reduces to 40.3ms, further demonstrating the efficiency of our approach in maintaining high accuracy while achieving low-latency control.

Overall, the ablations confirm that R3DP enhances 3D perception, multi-view fusion, and temporal reasoning, while preserving real-time efficiency.

5.4 Real-world experiments

Environments. We evaluate the practical applicability and geometric robustness of R3DP on a bimanual robotic system consisting of two ArmBot-Y1 arms and two fixed RealSense D435 cameras. We select two representative 3D-aware tasks for evaluation: *Place Shoe* and *Place Glass Cup*. These tasks are challenging due to the noisy and incomplete point clouds typically generated by consumer-grade depth sensors (As visualized in Figure 5), which often degrade the performance of point-cloud-based policies like DP3. Furthermore, to test environmental robustness, we conduct unimanual (single-arm) robot evaluations in a cluttered environment with significant lighting interference, featuring the *Pick Peach* and *Stack Bowls* tasks.

To ensure a fair and rigorous comparison, we train policies on 100 demonstrations for bimanual tasks and 50 for single-arm tasks. All models are validated across 30 independent trials under identical task configurations, with inference performed on a single NVIDIA RTX 4090 to assess success rates and latency.

Implementation Details. For real-world DP3 deployment, we crop out points corresponding to walls and background from the depth map, downsample it to 4096 points (as visualized in Figure 5), discarding color information to follow the original setting. All strategies use DDIM as the noise scheduler, with 100 steps during training and 10 steps during denoising.

Results. As shown in Table 4, R3DP significantly outperforms Diffusion Policy (DP) and DP3 by average margins of 40.9% and 23.3%, respectively. While DP3 relies on point clouds, which are often noisy and incomplete in real-world settings (as illustrated in Figure 5), our proposed VGGT and MVFF modules provide superior geometric perception, leading to more stable manipulation.

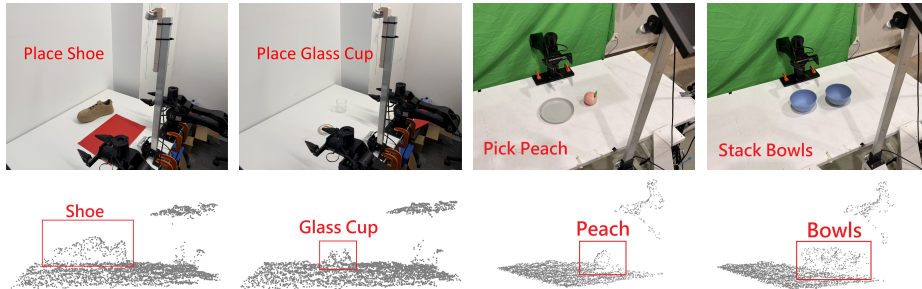


Fig. 5: Real-world experimental platforms and point cloud inputs. We evaluate our method on the ArmBot-Y1 bimanual robot for tasks including Place Shoe and Place Glass Cup, and a single-arm robot for Pick Peach and Stack Bowls. Both platforms are equipped with dual RealSense D435 cameras to generate the ground-truth point clouds used by the DP3 baseline.

Table 4: Real-world performance and inference latency. V and M denote VGGT and MVFF. For model training, we collect 100 episodes for dual-arm tasks and 50 episodes for single-arm tasks, respectively. All models are subsequently evaluated over 30 trials per task to report the success rates. For DP3, point cloud conversion introduces additional computational overhead.

Task (SR \uparrow)	DP	DP3	DP+V+M	R3DP
Place Shoe	46.7%	50.0%	76.7%	86.7%
Place Glass Cup	23.3%	56.7%	76.7%	83.3%
Pick Peach(Single Arm)	20%	30%	46.7%	50%
Stack Bowls(Single Arm)	33.3%	56.7%	66.7%	66.7%
Average	30.8%	48.4%	66.7%	71.7%
Latency (ms \downarrow)	<i>Inference Breakdown (RTX 4090)</i>			
Obs. Encoder	—	57.24	105.1	62.18
Action Expert	67.94	58.77	66.32	69.78

Furthermore, we analyze the inference efficiency on an NVIDIA RTX 4090 GPU. Although the inclusion of VGGT initially introduces an encoding bottleneck (105.1 ms), our optimized R3DP architecture reduces the observation encoding latency to 62.18 ms—nearly on par with DP (57.24 ms) while delivering higher success rates. This balance of efficiency and accuracy demonstrates R3DP’s readiness for real-time, high-performance 3D manipulation.

6 Conclusion

We presented R3DP, a real-time 3D-aware policy for embodied manipulation that injects strong 3D priors from large 3D vision models into standard image-based imitation policies. This framework is plug-and-play and can be instantiated on different policy backbones. Experiments show that R3DP substantially improves success rates over multiple baselines while maintaining real-time control. We believe this offers a promising path toward combining large-scale 3D models with fast control, and plan to extend R3DP to more contact-rich, long-horizon, and reinforcement-learning-driven manipulation.

References

1. Abouzeid, A., Mansour, M., Sun, Z., Song, D.: Geoaware-vla: Implicit geometry aware vision-language-action model. arXiv preprint arXiv:2509.14117 (2025)
2. Black, K., Brown, N., Darpinian, J., Dhabalia, K., Driess, D., Esmail, A., Equi, M.R., Finn, C., Fusai, N., Galliker, M.Y., et al.: π 0.5: a vision-language-action model with open-world generalization. In: 9th Annual Conference on Robot Learning (2025)
3. Black, K., Brown, N., Driess, D., Esmail, A., Equi, M., Finn, C., Fusai, N., Groom, L., Hausman, K., Ichter, B., et al.: π 0: A vision-language-action flow model for general robot control. arXiv preprint arXiv:2410.24164 (2024)
4. Cabon, Y., Stofl, L., Antsfeld, L., Csurka, G., Chidlovskii, B., Revaud, J., Leroy, V.: Must3r: Multi-view network for stereo 3d reconstruction. In: CVPR. pp. 1050–1060 (2025)
5. Chen, T., Chen, Z., Chen, B., Cai, Z., Liu, Y., Liang, Q., Li, Z., Lin, X., Ge, Y., Gu, Z., et al.: Robotwin 2.0: A scalable data generator and benchmark with strong domain randomization for robust bimanual robotic manipulation. arXiv preprint arXiv:2506.18088 (2025)
6. Chi, C., Xu, Z., Feng, S., Cousineau, E., Du, Y., Burchfiel, B., Tedrake, R., Song, S.: Diffusion policy: Visuomotor policy learning via action diffusion. *The International Journal of Robotics Research* **44**(10-11), 1684–1704 (2025)
7. Dinh Vuong, A., Nhat Vu, M., Reid, I.: Improving robotic manipulation with efficient geometry-aware vision encoder. arXiv e-prints pp. arXiv-2509 (2025)
8. Fang, X., Gao, J., Wang, Z., Chen, Z., Ren, X., Lyu, J., Ren, Q., Yang, Z., Yang, X., Yan, Y., Lyu, C.: Dens3r: A foundation model for 3d geometry prediction. arXiv preprint arXiv:2507.16290 (2025)
9. Feichtenhofer, C., Fan, H., Malik, J., He, K.: Slowfast networks for video recognition. In: Proceedings of the IEEE/CVF international conference on computer vision. pp. 6202–6211 (2019)
10. Gao, J., Wang, Z., Fang, X., Ren, X., Chen, Z., Liu, S., Cheng, Y., Lyu, J., Yang, X., Yan, Y.: More: 3d visual geometry reconstruction meets mixture-of-experts. arXiv preprint arXiv:2510.27234 (2025)
11. Gong, Z., Ding, P., Lyu, S., Huang, S., Sun, M., Zhao, W., Fan, Z., Wang, D.: Carp: Visuomotor policy learning via coarse-to-fine autoregressive prediction. In: Proceedings of the IEEE/CVF International Conference on Computer Vision. pp. 13460–13470 (2025)
12. Grotz, M., Shridhar, M., Chao, Y.W., Asfour, T., Fox, D.: Peract2: Benchmarking and learning for robotic bimanual manipulation tasks. In: CoRL 2024 Workshop on Whole-body Control and Bimanual Manipulation: Applications in Humanoids and Beyond (2024)
13. Jang, W., Weinzaepfel, P., Leroy, V., Agapito, L., Revaud, J.: Pow3r: Empowering unconstrained 3d reconstruction with camera and scene priors. In: CVPR. pp. 1071–1081 (2025)
14. Ke, T.W., Gkanatsios, N., Fragkiadaki, K.: 3d diffuser actor: Policy diffusion with 3d scene representations. arXiv preprint arXiv:2402.10885 (2024)
15. Leroy, V., Cabon, Y., Revaud, J.: Grounding image matching in 3d with mast3r. In: ECCV. vol. 15130, pp. 71–91 (2024)
16. Li, R., Yi, B., Liu, J., Gao, H., Ma, Y., Kanazawa, A.: Cameras as relative positional encoding. arXiv preprint arXiv:2507.10496 (2025)

17. Lin, T., Li, G., Zhong, Y., Zou, Y., Zhao, B.: Evo-0: Vision-language-action model with implicit spatial understanding. arXiv preprint arXiv:2507.00416 (2025)
18. Lin, X., Lin, T., Huang, L., Xie, H., Jin, Y., Li, K., Su, Z.: Sem: Enhancing spatial understanding for robust robot manipulation. arXiv preprint arXiv:2505.16196 (2025)
19. Liu, S., Wu, L., Li, B., Tan, H., Chen, H., Wang, Z., Xu, K., Su, H., Zhu, J.: Rdt-1b: a diffusion foundation model for bimanual manipulation. arXiv preprint arXiv:2410.07864 (2024)
20. Lu, Y., Tian, Y., Yuan, Z., Wang, X., Hua, P., Xue, Z., Xu, H.: H³dp: Triply-hierarchical diffusion policy for visuomotor learning. arXiv preprint arXiv:2505.07819 (2025)
21. Ma, J., Qin, Y., Li, Y., Liao, X., Guo, Y., Zhang, R.: Cdp: Towards robust autoregressive visuomotor policy learning via causal diffusion. arXiv preprint arXiv:2506.14769 (2025)
22. Manuelli, L., Gao, W., Florence, P., Tedrake, R.: kpm: Keypoint affordances for category-level robotic manipulation. In: The International Symposium of Robotics Research. pp. 132–157 (2019)
23. Miyato, T., Jaeger, B., Welling, M., Geiger, A.: Gta: A geometry-aware attention mechanism for multi-view transformers. arXiv preprint arXiv:2310.10375 (2023)
24. Nair, S., Rajeswaran, A., Kumar, V., Finn, C., Gupta, A.: R3m: A universal visual representation for robot manipulation. arXiv preprint arXiv:2203.12601 (2022)
25. Oquab, M., Darcet, T., Moutakanni, T., Vo, H., Szafraniec, M., Khalidov, V., Fernandez, P., Haziza, D., Massa, F., El-Nouby, A., et al.: Dinov2: Learning robust visual features without supervision. arXiv preprint arXiv:2304.07193 (2023)
26. O’Neill, A., Rehman, A., Maddukuri, A., Gupta, A., Padalkar, A., Lee, A., Pooley, A., Gupta, A., Mandlekar, A., Jain, A., et al.: Open x-embodiment: Robotic learning datasets and rt-x models: Open x-embodiment collaboration 0. In: 2024 IEEE International Conference on Robotics and Automation (ICRA). pp. 6892–6903. IEEE (2024)
27. Pearce, T., Rashid, T., Kanervisto, A., Bignell, D., Sun, M., Georgescu, R., Macua, S.V., Tan, S.Z., Momennejad, I., Hofmann, K., et al.: Imitating human behaviour with diffusion models. arXiv preprint arXiv:2301.10677 (2023)
28. Qian, Q., Zhao, G., Zhang, G., Wang, J., Xu, R., Gao, J., Zhao, D.: Gp3: A 3d geometry-aware policy with multi-view images for robotic manipulation. arXiv preprint arXiv:2509.15733 (2025)
29. Shridhar, M., Manuelli, L., Fox, D.: Perceiver-actor: A multi-task transformer for robotic manipulation. In: Conference on Robot Learning. pp. 785–799. PMLR (2023)
30. Shukor, M., Aubakirova, D., Capuano, F., Kooijmans, P., Palma, S., Zouitine, A., Aractingi, M., Pascal, C., Russi, M., Marafioti, A., et al.: Smolvla: A vision-language-action model for affordable and efficient robotics. arXiv preprint arXiv:2506.01844 (2025)
31. Tang, Z., Fan, Y., Wang, D., Xu, H., Ranjan, R., Schwing, A., Yan, Z.: Mv-dust3r+: Single-stage scene reconstruction from sparse views in 2 seconds. In: CVPR. pp. 5283–5293 (2025)
32. Wang, H., Agapito, L.: 3d reconstruction with spatial memory. In: 3DV (2025)
33. Wang, J., Chen, M., Karaev, N., Vedaldi, A., Rupprecht, C., Novotny, D.: Vggt: Visual geometry grounded transformer. In: CVPR (2025)
34. Wang, Q., Zhang, Y., Holynski, A., Efros, A.A., Kanazawa, A.: Continuous 3d perception model with persistent state. In: CVPR (2025)

35. Wang, S., Leroy, V., Cabon, Y., Chidlovskii, B., Revaud, J.: Dust3r: Geometric 3d vision made easy. In: CVPR. pp. 20697–20709 (2024)
36. Wang, Y., Zhou, J., Zhu, H., Chang, W., Zhou, Y., Li, Z., Chen, J., Pang, J., Shen, C., He, T.: π^3 : Scalable permutation-equivariant visual geometry learning. arXiv preprint arXiv:2507.13347 (2025)
37. Yang, J., Sax, A., Liang, K.J., Henaff, M., Tang, H., Cao, A., Chai, J., Meier, F., Feiszli, M.: Fast3r: Towards 3d reconstruction of 1000+ images in one forward pass. In: CVPR (2025)
38. Yang, L., Kang, B., Huang, Z., Xu, X., Feng, J., Zhao, H.: Depth anything: Unleashing the power of large-scale unlabeled data. In: Proceedings of the IEEE/CVF Conference on Computer Vision and Pattern Recognition. pp. 10371–10381 (2024)
39. Yang, L., Kang, B., Huang, Z., Zhao, Z., Xu, X., Feng, J., Zhao, H.: Depth anything v2. *Advances in Neural Information Processing Systems* **37**, 21875–21911 (2024)
40. Ze, Y., Chen, Z., Wang, W., Chen, T., He, X., Yuan, Y., Peng, X.B., Wu, J.: Generalizable humanoid manipulation with 3d diffusion policies. arXiv preprint arXiv:2410.10803 (2024)
41. Ze, Y., Zhang, G., Zhang, K., Hu, C., Wang, M., Xu, H.: 3d diffusion policy: Generalizable visuomotor policy learning via simple 3d representations. In: Proceedings of Robotics: Science and Systems (RSS) (2024)
42. Zeng, A., Florence, P., Tompson, J., Welker, S., Chien, J., Attarian, M., Armstrong, T., Krasin, I., Duong, D., Wahid, A., et al.: Transporter networks: Rearranging the visual world for robotic manipulation. arXiv preprint arXiv:2010.14406 (2020)
43. Zhang, J., Herrmann, C., Hur, J., Jampani, V., Darrell, T., Cole, F., Sun, D., Yang, M.H.: Monst3r: A simple approach for estimating geometry in the presence of motion. In: ICLR (2025)
44. Zhang, S., Wang, J., Xu, Y., Xue, N., Rupperecht, C., Zhou, X., Shen, Y., Wetstein, G.: Flare: Feed-forward geometry, appearance and camera estimation from uncalibrated sparse views. In: CVPR (2025)
45. Zhao, T.Z., Kumar, V., Levine, S., Finn, C.: Learning fine-grained bimanual manipulation with low-cost hardware. arXiv preprint arXiv:2304.13705 (2023)

A Simulation Task Description

We evaluate our method on 10 tasks in the RoboTwin benchmark, 9 of which follow the benchmark’s predefined task suite. The language description can be found in Table A.

Table A: Descriptions of the RoboTwin manipulation tasks and our additional Tube Insert task. Max Frames denotes the maximum number of frames used to determine whether an evaluation is considered a failure.

Task	Max Frames	Description
Bottle Adjust	400	Pick up the bottle on the table headup with the correct arm.
Block Hammer Beat	400	There is a hammer and a block on the table, use the arm to grab the hammer and beat the block.
Shoe Place	450	Use one arm to grab the shoe from the table and place it on the mat.
Container Place	350	Place the container onto the plate.
Dual Shoes Place	600	Use both arms to pick up the two shoes on the table and put them in the shoebox, with the shoe tip pointing to the left.
Diverse Bottles Pick	400	Pick up one bottle with one arm, and pick up another bottle with the other arm.
Block Handover	600	Use the left arm to grasp the red block on the table, handover it to the right arm and place it on the blue pad.
Put Apple Cabinet	600	Use arm movement to open cabinet and grab apple, then place apple inside and close cabinet.
Blocks Stack Easy	600	Place the black block on top of the red block at the center.
Tube Insert	500	Pick up tube and place it into container using arm movement.

A.1 Tube Insert Task Details

In order to specifically assess the capability of R3DP in manipulating transparent objects, we introduce a customized simulated task Tube Insert in addition to the pre-defined tasks in RoboTwin. A visualization of *Tube Insert* in simulation can be found in Fig. A.



Fig. A: The head and front camera view of Tube Insert task.

Task Setup. The background and lighting conditions of the *Tube Insert* task are consistent with those defined in the RoboTwin benchmark. Three custom objects are placed on the tabletop: a test-tube rack, a white rectangular plastic container with a grid pattern, and a transparent glass tube positioned inside the container.

Example Procedure. 1) The gripper first moves to a position 10 cm above the tube. 2) It approaches the tube and lifts it vertically by 4 cm. 3) The gripper then retracts and rotates to an upright orientation, ensuring that the tube opening faces upward. 4) Next, it moves to a position 20 cm above the target slot on the test-tube rack. 5) The gripper descends, inserts the tube into the rack, and releases it.

Success Criterion. Within 500 frames, the tube must be transported such that its final position is within 5 cm of the designated target location inside the test-tube rack along all three spatial axes.

B Real-world Task Description

B.1 Experiment Environment Settings

To evaluate the robustness of R3DP, we conducted real-robot experiments across two distinct experimental setups (Fig. B):

- Setting A (Controlled Indoor Environment): This setting is in a windowless, confined room. Fully controllable illumination. Clean white wall and tabletop. Two Armbot-Y1 robotic arms are positioned in parallel 60 cm from each other. Visual inputs are captured by two Intel RealSense D435 cameras, designated the front-view and head-view cameras, respectively. Specifically, the front-view camera is centered between the bases of the two manipulators. The head-view camera is mounted 80 cm directly above the front-view camera, maintaining a 60-degree downward tilt.
- Setting B (Open Laboratory Environment): This setting is in a wide laboratory. Subject to ambient natural light and semi-controlled artificial lighting. Clean white tabletop against a green-screen background. A single Armbot-Y1 arm is employed for these tasks. While the relative spatial transformation between the two cameras remains identical to Setting A, the camera rig is repositioned 90 cm in front of the robotic arm. In this configuration, the cameras face the manipulator instead of being co-directional with the end-effector to mitigate self-occlusion during single-arm manipulation.

B.2 Data Collection

As shown in Fig. C, we designated specific positions for data collection based on the head view. All positions were determined from head-view images without precise metric calibration.



Fig. B: Real-world experiment settings and tasks. The first two images correspond to Setting A, while the last two represent Setting B.

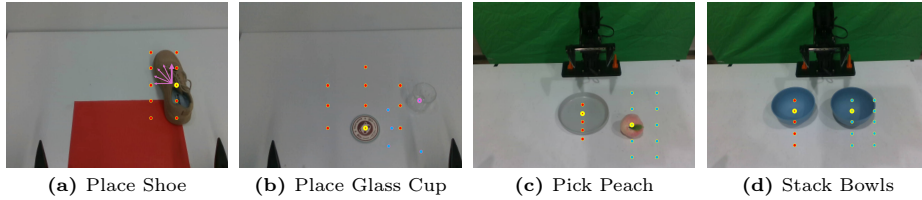


Fig. C: Real-world experiment data collection settings. Different colors represent different objects. The yellow edge means absolute position, and magenta means relative position or direction. The highlighted points represent the selected placement positions of the objects in the sample images.

- *Place Shoe*: We selected ten positions for the midpoint of the shoe. For each position, the direction of the shoe tip was uniformly divided into five intervals, ranging from the front to a direction perpendicular to the front and facing the centerline. Symmetric configurations were handled analogously. In all training data, the gripper was constrained to grasp the outer side of the shoe.
- *Place Glass Cup*: We selected ten positions for the midpoint of the coaster. For each coaster position, the cup was placed at five distinct relative locations: three closer and two farther. Symmetric configurations were handled analogously. In all training data, the gripper was constrained to grasp the outer side of the cup.
- *Pick Peach*: We selected five positions for the plate and ten positions for the peach. In all training data, the peach leaf was oriented toward the camera to ensure visual consistency.
- *Stack Bowls*: We selected five positions for the left bowl (fixed) and ten positions for the right bowl (to be moved). In all training data, the gripper was constrained to grasp only the right side of the bowl according to the camera view.

B.3 Detailed Evaluation Results

During our evaluation, we observed that different models fail in different cases. As shown in Table B, instead of a binary success/failure metric, we introduced

Table B: Detailed categorization of failure modes across four real-world tasks.

Task	Notation	Description
Place Shoe	Success	1 - Successfully placed the shoe inside the red area horizontally.
	Failure	0 - Failed to grasp. 2 - Placed the shoe out of the area or in incorrect orientation.
Place Glass Cup	Success	1 - Successfully placed glass cup fully onto the coaster.
	Failure	0 - Failed to grasp. 2 - Placed the glass cup out of the coaster.
Pick Peach	Success	1 - Successfully placed the peach onto the plate.
	Failure	0 - Attempted to grasp at the wrong position. 2 - Approached the correct position but failed to grasp. 3 - Placed the peach out of the plate.
Stack Bowls	Success	1 - Successfully stacked the right bowl onto the left one.
	Failure	0 - Attempted to grasp at the wrong position. 2 - Approached the correct position but failed to grasp. 3 - Placed the right bowl out of the left bowl or knocked it over.

Table C: Detailed real-world evaluation results

Task	DP	DP3	DP+VGGT	R3DP
Place Shoe	1012011100	0100100110	1111102121	1111111111
	1110112000	1100112101	1011101110	1112111111
	1000011210	1011020211	1111111110	1221111211
Place Glass Cup	1010000011	1000010100	1110111110	1110111111
	0000000001	1111010111	1111000111	1112111112
	2010010020	1001011011	0111110111	1121110111
Pick Peach	0022212211	1000110110	1100211100	0112210110
	0203010021	2000002001	2121131210	2211111201
	0220013022	0001021010	1100120010	1101200100
Stack Bowls	1221030321	3113111001	1001133111	1100111333
	3221123231	1313031311	1311021311	0111131131
	2212211212	1133113011	2111131111	1211111112

a fine-grained categorization of failure modes to discuss the performance of different models. Based on the categorization, we listed detailed evaluation results in Table C.

C Full Experiments on Different τ

In our framework, τ is a hyperparameter that controls the interval between two queries to the slow branch. In the main paper, we report results with $\tau = 4$ and $\tau = 8$. In Table D, we provide the complete experimental results under a wider range of τ values, including $\tau = 2, 4, 8, 16,$ and 32 . To assess the sensitivity of our framework to this hyperparameter, we report the average success rate and the corresponding standard deviation across all tasks for each τ configuration.

Table D: Performance under different values of the hyperparameter τ .

Task	$\tau = 2$	$\tau = 4$	$\tau = 8$	$\tau = 16$	$\tau = 32$	Average
Block Hammer Beat	60%	77%	77%	87%	85%	77.2% \pm 9.52%
Block Handover	75%	95%	93%	93%	90%	89.2% \pm 7.28%
Bottle Adjust	56%	62%	56%	53%	53%	56.0% \pm 3.29%
Blocks Stack Easy	64%	69%	72%	67%	69%	68.2% \pm 2.64%
Shoe Place	73%	72%	68%	74%	61%	69.6% \pm 4.76%
Container Place	50%	63%	54%	57%	53%	55.4% \pm 4.41%
Dual Shoes Place	20%	24%	20%	21%	19%	20.8% \pm 1.72%
Diverse Bottles Pick	28%	31%	32%	34%	33%	31.6% \pm 2.06%
Put Apple Cabinet	100%	100%	99%	100%	100%	99.8% \pm 0.40%
Tube Insert	90%	97%	97%	98%	99%	98.0% \pm 0.89%

Table E: Inference latency for each τ .

Latency (ms)	$\tau=2$	$\tau=4$	$\tau=8$	$\tau=16$	$\tau=32$
Obs. Encoder	66.17	50.52	40.27	33.31	31.04
Action Expert	54.35	55.27	56.66	51.83	52.25

D Implementation Details

In this section, we provide additional implementation details of R3DP used in all our experiments. We first outline the overall training pipeline, highlighting the two-stage design that decouples 3D feature distillation from policy learning. We then describe the pre-training setup of the Temporal Feature Prediction Network (TFPNet) and the training details of R3DP for both RoboTwin simulation and real-world experiments respectively, covering their training paradigms, data sampling strategies, and optimization hyperparameters. The training protocols and hyperparameters are the same for both simulation and real-world experiments. The difference lies only in the training data source and evaluation environment.

D.1 Overall Training Pipeline

Our training follows a two-stage pipeline. In the first stage, we pre-train the Temporal Feature Prediction Network (TFPNet) using supervision from a frozen VGGT backbone, learning to predict 3D-aware features across multi-view manipulation trajectories. In the second stage, we integrate TFPNet into the AFSC module for policy training, where VGGT and TFPNet process frames at different temporal rates. The R3DP policy is then trained end-to-end, with both VGGT and TFPNet frozen during this phase.

D.2 TFPNet Pre-training Details

The TFPNet is trained independently for each task using a sequence-based learning approach. For RoboTwin simulation, the dataset consists of approximately 200,000 sequences per task from the same 100 trajectories used for imitation learning, with each sequence containing 4 consecutive frames captured from two different camera views, head and front. For real-world experiments, we use the

same model architecture and training protocol, while the training data are constructed from the collected real-world demonstrations described in Sec. B.2. For each task, we train a separate model using a dataset constructed solely from the sequences of that task.

During pre-training, we freeze the VGGT encoder, and only optimize the parameters of the TFPNet. For each sequence, we extract intermediate VGGT tokens as supervision targets and let TFPNet iteratively predict the corresponding features over time, starting from the ground-truth features of the first frame. The training loss is given by a sequence feature-matching objective, while depth reconstruction is used for validation and optional visualization but is not included in the training objective.

The full set of optimization and data-loading hyperparameters is summarized in Table F.

Table F: TFPNet training hyperparameters.

Parameter	Value
sequence_length	4
num_views	2 (head, front)
image_size	308×168
batch_size	12
accumulation_steps	1
optimizer.lr	1.0×10^{-4}
optimizer.betas	(0.9, 0.999)
optimizer.eps	1.0×10^{-8}
optimizer.weight_decay	1.0×10^{-4}
num_epochs	100
gradient_clip_norm	1.0
mixed_precision_dtype	bfloat16
gradient_accumulation_steps	1
gpu	8×NVIDIA A800
per_task_sequences	200,000

Table G: R3DP Training hyperparameters.

Parameter	Value
horizon	8
n_obs_steps	1
n_action_steps	8
n_latency_steps	0
num_inference_steps	100
obs_as_global_cond	True
dataloader.batch_size	8
dataloader.num_workers	0
dataloader.shuffle	True
dataloader.pin_memory	True
dataloader.persistent_workers	False
optimizer_target_	torch.optim.AdamW
optimizer.lr	2.0×10^{-5}
optimizer.betas	(0.95, 0.999)
optimizer.eps	1.0×10^{-8}
optimizer.weight_decay	1.0×10^{-6}
gradient_clip_norm	1.0
training.lr_scheduler	cosine
training.lr_warmup_steps	500
training.num_epochs	600
training.gradient_accumulate_every	1
training.use_ema	True
training.max_grad_norm	1.0
gpu	8×NVIDIA RTX 4090

D.3 R3DP Policy Training Details

We adopt Diffusion Policy (DP) as the underlying visuomotor backbone and replace its original visual encoder with our 3D-aware perception encoder, which consists of the AFSC module, the pre-trained TFPNet, and the MVFF module. During policy training, both the VGGT encoder and the pretrained TFPNet remain frozen. Only the diffusion policy backbone is updated. Each training sample is a short trajectory segment consisting of 8 frames that are uniformly spaced by a stride of 8 control steps, resulting in an effective temporal window of 64 steps. For each frame, we use both head and front camera images together with

proprioceptive states as the observation, and condition the diffusion denoiser on the fused 3D-aware features produced by R3DP. During policy training, the diffusion denoiser is conditioned on the same AFSC-generated features as used at inference time: VGGT features are computed on sparse key frames, while features for the remaining frames are provided by the frozen TFPNet.

We train a separate policy for each task using the same training configuration. This protocol is shared by both RoboTwin simulation and real-world experiments. The training hyperparameters are summarized in Table G.

D.4 Details for Baselines and Ablation Variants

To ensure a fair comparison, all Diffusion-Policy-based baselines and ablations are trained using the same demonstration sets, action horizon, and optimization hyperparameters as our full R3DP model (see Table G). For each method, we evaluate checkpoints at 300, 450, and 600 epochs under identical settings and report the best-performing checkpoint in the main tables. The architectural definitions of DP-single, DP-multi, DP+VGGT, DP+VGGT+MVFF, and R3DP with AFSC strictly follow the descriptions in the main paper, and no additional tuning beyond the shared configuration is applied.

Finally, to help readers better understand the structure of MVFF and its corresponding ablation, we provide simplified PyTorch-style pseudocode for both modules as follows.

```

1 # Fusion; set geom=False for ablation w/o MVFF
2 class Fusion(nn.Module):
3     def forward(self, view_tokens, Ks=None, Tcw=None, geom=True):
4         x = flatten(view_tokens)
5         q, k, v = proj(x)
6         if geom:
7             # MVFF: PRoPE + cam geo
8             cam = flatten_cam(Ks, Tcw)
9             a = prope_attn(to_heads(q,k,v), cam)
10        else:
11            # Abl.: standard dot-product attention
12            a = sdpa(to_heads(q,k,v))
13        y = from_heads(a)
14        return unflatten(y)

```